Multi-Band Vehicle-to-Vehicle Channel Characterization in the Presence of Vehicle Blockage

MATE BOBAN[1], **DIEGO DUPLEICH**[2], **NAVEED IQBAL**[1,2], **JIAN LUO**[1],
CHRISTIAN SCHNEIDER[2], **ROBERT MÜLLER**[2], **ZIMING YU**[1],
DAVID STEER[1], **(Life Member, IEEE)**, **TOMMI JÄMSÄ** [1],
JIAN LI[1], **AND REINER S. THOMÄ**[2], **(Fellow, IEEE)**
[1]Huawei Technologies Duesseldorf GmbH, Riesstrasse 25, 80992 Munich, Germany
[2]Institute for Information Technology, Technische Universität at Ilmenau, D-98684 Ilmenau, Germany

Corresponding author: Mate Boban (mate.boban@huawei.com)

ABSTRACT Vehicle-to-vehicle (V2V) channels exhibit unique properties due to the highly dynamic environment and low elevation of the antennas at both ends of the link. Of particular importance for the behavior of V2V channels, and consequent reliability of the communication link, is the severity and dynamics of blockage of both the line-of-sight and other multipath components (MPCs). The characteristics of blockage become more important as the carrier frequency increases, and the ability of the signal to penetrate through objects diminishes. To characterize the effects of vehicle blockage, we performed V2V channel measurements in four different frequency bands (6.75, 30, 60, and 73 GHz) in urban and highway scenarios. We analyzed the impact of the blocker size and position on the received power and fast fading parameters, as well as the frequency dependence of these parameters under blockage. Our results show that there is a strong influence of the size of the blocking vehicle on the blockage loss and the angular/delay spread. The position of the blocker relative to the transmitter and receiver also plays an important role. On the other hand, the frequency dependence is quite limited, with the blockage loss increasing slightly and the number of scattered MPCs reducing slightly as frequency increases. The main conclusion of this paper is that V2V communication will be possible in high (millimeter-wave) frequencies, even in the case of blockage by other vehicles.

INDEX TERMS V2V, channel modeling, mmWave, cmWave, multi-band measurements, blockage.

I. INTRODUCTION

Vehicle to everything (V2X) communications have been envisioned to enable ever more advanced use cases, ranging from platooning, emergency lane change, overtaking assistance, to sensor sharing [1], ultimately leading to cooperative automated driving [2]. Because these use cases require a combination of low latency and high reliability, V2X is one of the most challenging ''verticals'' that cellular network is envisioned to support. Furthermore, the stringent requirements and close proximity of vehicles interacting with each other often make direct vehicle-to-vehicle (V2V) communications the best way to ensure successful execution of a use case. V2V propagation channels are considered to be more cluttered as compared to the conventional channels known from the cellular communications. The reasons include low (near to the ground level) antenna heights, severe blockage

effects by the surrounding vehicles, location of the antenna at the vehicle, and mobility of both transmitter (TX) and the receiver (RX) [3]. These characteristics distinguish the V2V channels from other types of mobile channels and present unique challenges for their measurement and modeling.

The previous work on V2V channel measurement and modeling has been heavily focused on bands around the 5.9 GHz, largely motivated by an allocated frequency band at that frequency for road safety and traffic efficiency applications in key markets (e.g., U.S. and Europe). The survey papers [3]–[5] provide a detailed overview of the V2V channel measurements and modeling research below 6 GHz. The studies in [6]–[12], along with many others mentioned in [3]–[5], provide the empirical path-loss and shadow fading models based on the joint statistics of LOS and non-LOS (NLOS) measurement samples.

Other measurements detailed in [10] and [13]–[19] describe the propagation losses at the street intersections. The studies in [20] and [21] analyze the impact of vehicles as propagation path blockers and demonstrate a 5-25 dB vehicle blockage loss at the 5.9 GHz frequency band. Abbas et al. [22] proposed a shadow fading model which takes vehicles blockage loss into account. Nilsson et al. [23] developed and evaluated through measurements a shadowing model that addresses the correlated shadow fading of multiple collocated links. Blockage by surrounding vehicles also profoundly affects the fast fading parameters. The results reported in [24] show a root mean squared (rms) delay spread (DS) of up to 100 ns.

Recently, discussions have started on using additional frequency bands (either dedicated for traffic safety or controlled by operators) beyond 5.9 GHz, in particular to enable advanced V2X use cases. A recent 3GPP Study Item (SI) explored the regulatory requirements and design considerations of V2V communications in spectrum beyond 6 GHz [25]. This SI considered spectrum below and above 6 GHz, including millimeter wave (mmWave) bands (e.g., 63-64 GHz as allocated for traffic safety in Europe and 76-81 GHz). The study developed fairly simple V2V channel models for spectrum both below and above 6 GHz.

In contrast to the V2V channels below 6 GHz, much less is known about the V2V channels at the mmWave frequency bands. The omni-directional channel measurements at these frequencies are quite challenging due to the severe link budget issues. Most of the measurements e.g. [26]–[32], use directional horn antennas facing a particular direction (e.g., transmitter and receiver antennas facing each other) and are not intended to scan other directions. These measurements primarily aim to analyze the strength of the LOS directional link. Below is a summary of lessons learned from these measurements:

- Directional measurements at 38 GHz, 60 GHz and 76 GHz frequency bands [26]–[28] proposed a 2-taps tapped delay model (LOS followed by a reflected MPC).
- The measurements at the 28 GHz frequency band reported a maximum blockage loss of 20 dB [30], whereas the measurements in 60 GHz reported 5-30 dB vehicle blockage loss increase from light to intense traffic conditions [29], [31]. Furthermore, measurements in 36 GHz and 76 GHz frequency bands reported a 20 dB blockage loss due to a truck [32], [33], whereas the multiple-input-multiple-output (MIMO) measurements [34] at 15 GHz using the omni-directional antenna at the RX reported a 3-12 dB blockage loss caused by a garbage truck.
- The delay and angular spreads increase notably in case of vehicle blockage. For example, the measurements at 28 GHz frequency band reported in [35] showed that a passenger bus blocking LOS causes up to 40 ns increase in the root mean squared delay spread and 20° increase in angular spread. Other studies show similar results (e.g., [29], [31]).

However, recent studies showed that, irrespective of the frequency, V2V channels experience frequent and significant non-LOS conditions, with the average blocking duration on the order of seconds to minutes [36], [37]. To our best knowledge, beyond our initial work on the topic [38], there is no existing work that compares the properties of the full omni-directional V2V propagation channels of the frequencies above 5.9 GHz. In addition to the LOS path, a propagation channel may also exhibit reflected, diffracted and scattered (diffuse) MPCs. Statistically, the situations when all the MPCs are completely blocked or obstructed at the RX occur rarely. If a certain path is blocked/obstructed, the communication may still be possible due to other MPCs. Therefore, to design a reliable V2V communication system, an in-depth characterization of the omni-directional channel is crucial. In this work, we aim to fill this gap by performing simultaneous Ultra-Wide Band (UWB) channel measurements at 6.75 GHz (3.4–10.1 GHz), 30 GHz (30.4–37.1 GHz) and 60 GHz (57.4–64.1 GHz) bands in an urban street canyon scenario. These bands are of particular importance because they encompass current band allocations for V2V (e.g., 5.9 GHz band allocated for traffic safety in the U.S. and Europe and 63-64 GHz band allocated in Europe) as well as possible future bands (e.g., around 30 GHz in U.S. and Asian markets, either in licensed operator bands or as unlicensed traffic safety bands). For each frequency band, the analysis highlights the properties of the composite signal at RX (i.e., considering all MPCs), including signal strength variations and dispersion statistics when a LOS path between the TX and RX vehicles is obstructed by overtaking vehicles of different sizes. For the comparison purpose, we also report the results from the 73 GHz directional channel measurements in highway and urban scenarios. The discussions on the small scale fading have been intentionally avoided as they are heavily influenced by the system properties such as bandwidth and antenna/beamforming gain. Such discussions are beyond the scope this work. For detailed analysis on the impact of the system assumptions on the radio channel properties, we refer the interested reader to our earlier work (e.g., [39], [40], and references therein).

II. MEASUREMENT SETUP AND SCENARIOS
This section contains a description of the measurement setup, environments, vehicles and equipment used in the measurements.

A. MULTIBAND OMNI-DIRECTIONAL STREET CANYON MEASUREMENTS IN ILMENAU URBAN
The measurements were carried out with a dual-polarized UWB multi-channel sounder (DP-UMCS) introduced in [41]. It offers, after back-to-back calibration, a null-to-null absolute bandwidth of 5.1 GHz enabling a high resolution in the delay domain and allows a better identification of scatterers in comparison to lower resolution sounding systems.
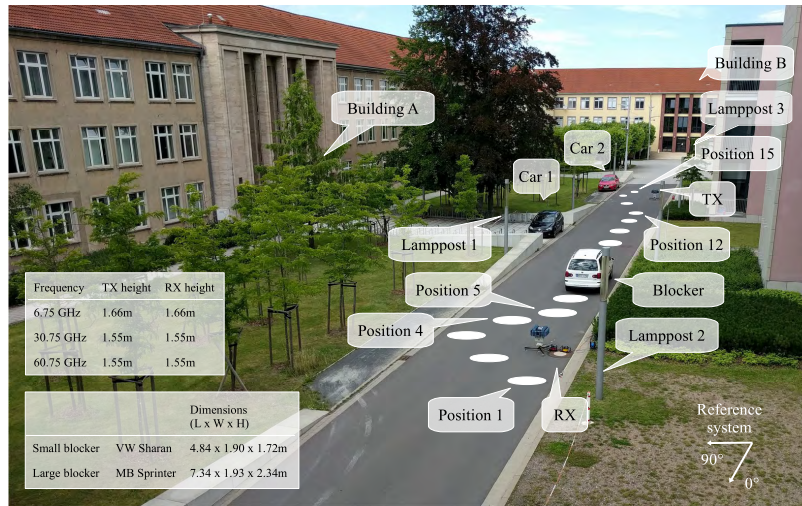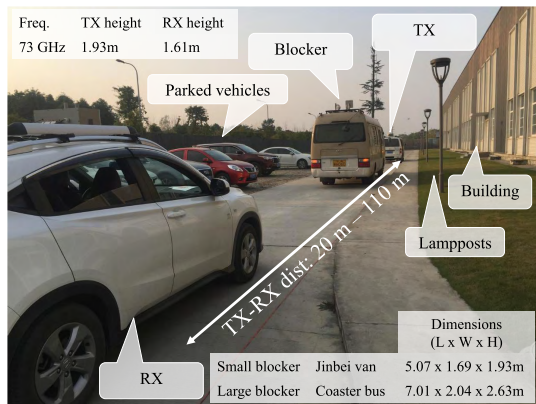
FIGURE 1. Measurement scenarios. For measurements in Ilmenau (a), TX and RX are mounted on poles. The distance between two neighboring positions of the blocking vehicle is around 2 m. For measurements in Chengdu, both urban and highway (b) and (c), respectively, TX and RX are mounted on rooftops of vehicles with following dimensions (L × W × H): 5.07 × 1.69 × 1.93 m (TX, Jinbei van); 4.27 × 1.77 × 1.61 m (RX, Honda XR-V).

The channel sounder configuration consists of a square head with antennas for the different frequency bands on the different sides. This multiband measurement procedure has been introduced in [42]. Dual polarized horn antennas with 30° half power beamwidth (HPBW) were used at both link ends to scan the environment in 360° in azimuth with 30° scan steps. The antenna patterns present similar characteristics in the angular domain in the different bands (information taken from datasheets and in-house measurements). However, since our measurements are wideband, the response of the antennas within the measured bandwidth might vary slightly from band to band. Hence, since the antennas were not de-embedded from the measurements, the results are still influenced by them. However, without the availability of multi-band antenna arrays and high-resolution parameter estimation algorithms for mmWaves, we believe our approach is the closest to simultaneous multi-band analysis that we can perform. Finally, for each measurement position, all the frequency bands are measured at the same time while maintaining nearly the same static environment for each band.

This set-up is a compromise between directional and mobility characterization of the environment, since it is not possible to measure aspects as Doppler. Furthermore, a camera mounted at the sounding system takes pictures during each directional scan of the rotating horn antennas. These pictures are then used to identify scattering objects in the environment.

The measurements were performed at the campus of the Technische Universität Ilmenau, Ilmenau, Germany. The scenario was a street canyon in an urban environment with parked cars, multi-story buildings, and lampposts as shown in Fig. 1(a). The TX and RX emulate two cars that are 44 m apart communicating to each other with antennas at a rooftop level with the heights shown in Fig. 1(a). Two parked cars (labeled as Car 1 and Car 2) were present during the measurements to increase the scattering effects. A third vehicle, labeled blocker, was positioned in 15 different locations (Position 1-15 in Fig. 1(a)), emulating an overtaking situation. This results in non-LOS condition due to vehicles (NLOSv) at Positions 5 to 12. In addition to

the 15 positions with the blocker vehicle, a reference scenario – without the blocking vehicle in the environment – was also measured. To analyze two typically occurring blocking scenarios, we performed measurements with two blocking vehicles: i) small blocker, represented by a passenger vehicle (Volkswagen Sharan), which was slightly taller than the TX and RX antennas of the sounding apparatus; and ii) large blocker, represented by a Mercedes Benz Sprinter van, which was approximately 80 cm taller than the TX and RX antennas. Fig.1(a) shows the details of the measurement setup, including the dimensions of vehicles. All the measurements were performed in as static scenario as possible by restricting the access of the streets.

B. 73 GHZ DIRECTIONAL CHANNEL MEASUREMENTS IN CHENGDU

The measurements were carried out at 73 GHz with a 614 MHz absolute bandwidth of the sounding system. Unlike the rotating horn antenna based technique used in the Ilmenau measurements, both the TX and RX of the sounding system used here are equipped with arrays of four 30° HPBW horn antennas enabling a total directional coverage of 120° in azimuthal space. During the measurements, both TX and RX antenna arrays are placed at the roof tops of vehicles with their boresights facing each other with a blocking vehicle in between as shown in Figs. 1(b) and 1(c).

1) URBAN:

The urban grid measurement was conducted on Huawei campus in Chengdu, China. As shown in Fig. 1(c), the street is lined with parked cars at one side and buildings (of 9 m height) on the opposite side. There are lampposts in front of the buildings and occasional foliage further away. Three measurement setups were defined: i) no vehicle blockage (LOS case); ii) small vehicle blocker case; and iii) large vehicle blocker case. In the LOS case, the TX position was static while the RX, which is initially 20 m away from the TX, was moved away from the TX in 2 m steps up to a distance of 110 m. The only difference between the vehicle blockage measurements to the LOS case was that a blocking vehicle is positioned in between the TX and RX at a fixed location 15 m away from the TX. In all the cases, the environment was kept as static as possible.

2) HIGHWAY:

The site of this measurement campaign is the Binghe road, Chengdu, China. The highway is a bi-directional eight lane road (four lanes per direction), which has a speed limit of 80 km/h. As shown in Fig. 1(c), the measurements were carried out at the right-most lane adjacent to the green belt with occasional trees, foliage, and a wall approximately 15 m away from the travel lane. Unlike the urban scenarios in Figs. 1(a) and 1(b), this measurement environment is more dynamic due to occasional traffic on the road during the measurement campaign. In the LOS case, the TX was placed at a fixed position. The RX, is starting at an initial

location 20 m away from the TX, was moved away along the lane in 8 m increments up-to a distance of 140 m. In the case of vehicle blockage measurements, the blocking vehicle (30m away from the TX) was placed at a fixed position between the TX and RX, whereby the RX (initially at 36m distance to the TX) was moved away along the lane in 8 m increments up to 140 m distance.

III. MEASUREMENT RESULTS AND ANALYSIS

In this section, we analyze the effect of the blocking vehicle by taking a closer look at the synthetic omni-directional power delay profile (PDP) at different positions of the blocker with respect to the TX and RX. Let θ_{TX} and θ_{RX} be the TX and RX antenna pointing angles when a signal is transmitted with a polarization a and received with a polarization b, where, $a, b \in \{H \text{ (Horizontal)}, V \text{ (Vertical)}\}$. Let P be the power an MPC arriving at the Rx at a delay τ_i then the synthesized omni-directional PDP is computed as the power summation at a delay τ_i along angular and polarization domain as

$$P_{\text{Syn. Omni}}(\tau_i) = \sum_{\forall a,b} \sum_{\forall \theta_{\text{TX}}} \sum_{\forall \theta_{\text{TX}}} P_{ab}(\tau_i, \theta_{\text{TX}}, \theta_{\text{RX}}) \cdot \quad (1)$$

The synthesized omni-directional PDPs from the directional channel sounding are widely accepted in the mmWave measured channel data analysis [43], [44]. We analyze the impact of the vehicle blockage loss and the RMS delay spread directly from the PDP obtained from Eq.(1).

A. DYNAMIC RANGE

The dynamic range (DR) is a difference in the power of the strongest to the weakest MPC in the PDP. In literature, the DR is often applied relative to the LOS path for all positions in the measurement ensemble. This may result in a reduced RMS DS in the NLOSv positions as demonstrated in [45]. In contrast, we have applied the DR independently at each measured position. In the post-processing, a noise floor n_f is estimated for each directional PDP using the procedure described in [46] and all delay samples below n_f are zeroed out. After that, a dynamic range of 30 dB is applied to the synthesized omni-directional PDP of the channel. This dynamic range is maintained at each measured frequency band in the LOS or NLOSv measurement positions. Note that the DR of the DP-UMCS system used in Ilmenau urban measurements is 70dB, which enables the identification of very weak MPCs. Due to the independent application of the DR at each measured position, the weaker MPCs in NLOSv positions are expected to contribute to the dispersion statistics resulting in higher delay and angular spreads than the LOS positions.

B. IMPACT OF VEHICLE BLOCKAGE ON THE POWER DELAY PROFILE

Analyzing the dynamics of V2V channel in the delay domain allows for an intuitive characterization of the vehicle blockage impact on the MPCs. Figs. 2(a) and 2(b) show the normalized synthetic omni-directional PDP for two adjacent

(b)
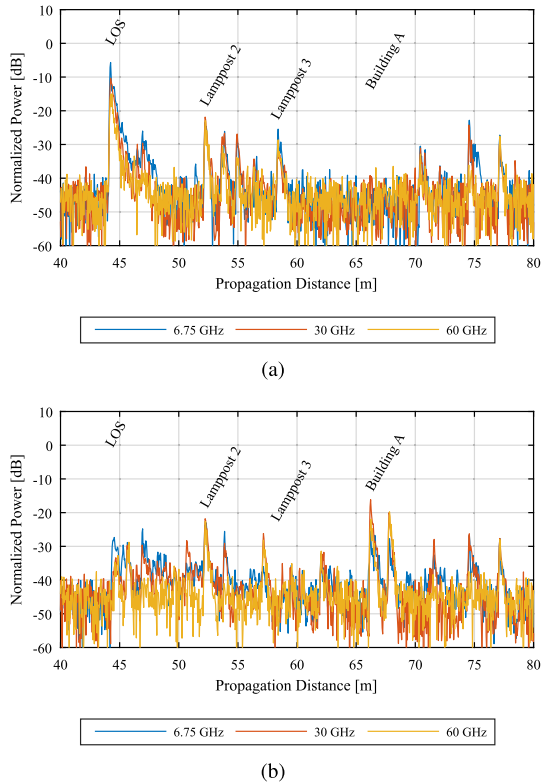
FIGURE 2. Comparison of synthetic omni-directional PDPs for two nearby locations of the blocker in Ilmenau Urban scenario with large blocker. PDP is normalized with respect to the LOS component of measurements without the blocking vehicle in any of the positions in Fig. 1(a). (a) Blocking vehicle in Position 4 (see Fig. 1(a)). (b) Blocking vehicle in Position 5 (see Fig. 1(a)).

positions (Position 4 and 5) of the blocking vehicle in the Ilmenau urban scenario (Fig. 1(a)). The PDPs in Fig. 2 have been normalized with respect to the power of LOS path (i.e. without obstruction). While the difference between two positions is only the movement of the blocking vehicle by about two meters, a difference in the LOS path obstruction results in fundamentally different PDPs in Fig. 2. The vehicle blockage results in more than 20 dB attenuation of the LOS path, thus making the reflections off the buildings (Building A in this example) and scattering off the lampposts (Lamppost 2 and 3) the dominant contributors of energy at the RX. Fig. 2 shows that the difference in the PDP resulting from LOS path blockage loss is quite comparable across frequencies, despite of the wavelength at 60 GHz band being about nine times shorter than at the 6.75 GHz band. Interestingly, at the blocker Position 5 (Fig. 2(b)), the reflection from the building A is roughly 10 dB lower than the LOS path in Position 4 (Fig. 2(a)) for all bands. This illustrates that communication in these bands may often be feasible even with blockage of the LOS path. Furthermore, while there are differences across the three frequency bands (centered at 6.75, 30, and 60 GHz), the dominant components are consistent across frequencies. In summary, the example in Fig. 2 shows how dynamic the V2V channel can be – with a single change in the underlying geometry, the resulting

channel changes considerably. However, even though the LOS path is blocked, the presence of other scattered MPCs from the environment indicate that the communication is still feasible at higher frequency bands.

C. IMPACT OF THE SIZE AND POSITION OF VEHICLE BLOCKER

Different types of vehicles (e.g., personal vehicles, commercial vans, trucks, scooters, and public transportation vehicles) have distinct dimensions and mobility dynamics. Therefore, a model for the propagation characteristics of one vehicle type is not directly applicable to other types. Furthermore, distinct features of vehicle types have an impact on the propagation modeling even if the vehicle itself is not the TX or the RX. For example, on highways, it is easy to imagine a platooning scenario where a vehicle in a platoon obstructs the LOS for other members of the platoon in front and behind it. Similarly, a passenger vehicle located in a lane behind a large truck is likely to experience strong attenuation when communicating to any vehicle in front of that truck. Motivated by such situations, in all three scenarios shown in Fig. 1, we performed measurements with both a small blocker and a large blocker, to allow for an analysis of the impact of the vehicle blocker size on V2V channels. Dimensions of blockers are shown in Fig. 1. Table 1 shows that the most obvious effect of increased blocker size is an increase in blocking loss. Across the measured scenarios, the additional attenuation that a larger blocker introduces on top of small blocker loss is 6 dB on average. In terms of absolute loss, it ranges from 4 dB (minimum average small blocker loss) to 17 dB (maximum average large blocker loss).

The measured DS per position for each location of the small and large blocker in the Ilmenau Urban scenario is shown in Figs. 3(a) and 3(b), respectively. While the largest difference is between positions with vehicle blockage (Position 5-12) and those without blockage (Position 1-4 and 13-15), the difference between small and large blocker is also noticeable, with the large blocker causing higher increase in the DS than the small blocker. Furthermore, when comparing Figs. 3(a) and 3(b) with their counterparts in terms of received power (Figs. 3(c) and 3(d), respectively), we can see a strong negative correlation between the DS and received power. The LOS positions show the lowest DS and highest power, whereas in the blocked positions DS increases considerably, while the RX power is reduced. We can also conclude that, in case of blocked LOS, the closer the vehicle blocker to TX or RX, the higher the DS and lower the received power, with the DS at the lowest value when the blocker is exactly in the middle between the TX and RX (Position 8). These results confirm that the larger and closer the blocker, the larger the number of dominant MPSs it shadows, which in turn reduces the overall power at the receiver, while increasing the delay spread of the channel. Fig. 3(a) shows that, with a small blocking vehicle, the DS values for different frequencies are quite similar. In contrast, with a large blocking vehicle in Fig. 3(b), there is a clear trend of increasing DS

TABLE 1. Multi-band fast-fading parameters for different scenarios. Note that the measurement campaigns at f_c = 6.75, 30, and 60 GHz are from Ilmenau Urban scenario, whereas campaigns at f_c = 73 GHz are from Chengdu scenarios.

			DS [ns]				ASA [Deg.]				ASD [Deg.]				Blocking Loss [dB]			
		f_c [GHz]→	6.75	30	60	73	6.75	30	60	73	6.75	30	60	73	6.75	30	60	73
			Synthesized Omni directional TX-RX															
Urban (Ilmenau)	LOS	Mean	19.7	19	16.3	-	28.5	27.3	19.7	-	29.7	26.9	19	-	N/A	N/A	N/A	-
		std.	3.5	5.7	6	-	5.7	6.6	7.7	-	8.7	6.6	10.6	-	N/A	N/A	N/A	-
	Non-LOS (small blocker)	Mean	33.3	35.8	32.5	-	37.3	39.5	34.8	-	32.2	34.1	30.1	-	5.5	6.3	8.2	-
		std	2.5	5.7	5.9	-	2.6	4.2	9	-	4.2	4.3	5.2	-	1.1	1.7	2.2	-
	Non-LOS (large blocker)	Mean	49	44	37.6	-	42	41.6	39.5	-	60	56.6	50.4	-	9.6	11	12.2	-
		std.	9.4	6.9	8.3	-	13	8.4	11.4	-	27.9	14.3	17.5	-	2.5	3	4	-
			Directional (120° HPBW) TX-RX															
Urban (Chengdu)	LOS	Mean	-	-	-	10.2	-	-	-	25.6	-	-	-	25.1	-	-	-	N/A
		std.	-	-	-	4.5	-	-	-	3.7	-	-	-	4.6	-	-	-	N/A
	Non-LOS (small blocker)	Mean	-	-	-	13	-	-	-	25	-	-	-	25.4	-	-	-	6
		std	-	-	-	5.8	-	-	-	3.8	-	-	-	5.4	-	-	-	5
	Non-LOS (large blocker)	Mean		-	-	12	-	-	-	25.6	-	-	-	27	-	-	-	8.2
		std.	-	-	-	4.6	-	-	-	8.2	-	-	-	9.5	-	-	-	4.1
Highway (Chengdu)	LOS	Mean	-	-	-	6.1	-	-	-	23.4	-	-	-	23	-	-	-	N/A
		std.	-	-	-	2.8	-	-	-	3.2	-	-	-	4.2	-	-	-	N/A
	Non-LOS (small blocker)	Mean	-	-	-	4.6	-	-	-	18.8	-	-	-	21.5	-	-	-	6.2
		std	-	-	-	2.7	-	-	-	6.7	-	-	-	6.2	-	-	-	4
	Non-LOS (large blocker)	Mean	-	-	-	8.1	-	-	-	15.8	-	-	-	13.6	-	-	-	17
		std.	-	-	-	6.6	-	-	-	8.2	-	-	-	10.1	-	-	-	6.7

with decreasing frequency. Finally, perhaps the most striking result we can discern from Figs. 3(c) and 3(d) is that *the normalized received power is similar across frequencies*, with at most 8 dB difference between received power at 6.75 GHz and 60 GHz in any of the positions. In Position 8 (blocker in the middle between TX and RX), due to the less obstructed Fresnel zone of the ground reflected ray in 30 GHz and 60 GHz, the normalized received power is even *higher than in 6.75 GHz*.

D. FREQUENCY AND DISTANCE DEPENDENCE OF VEHICLE BLOCKAGE LOSS

In this section, we assess if there is a measurable and consistent behavior of blockage loss at different frequencies. Establishing such a relationship between the blockage loss and frequency would enable a more accurate and efficient modeling of blockage loss. For example, in case the loss is frequency-dependent, it can be added to the path loss equation for LOS channel as a function of the carrier frequency (and, additionally, the type of blocker). The study on frequency dependency of blockage loss focuses on the Ilmenau Urban scenario, since it contains multi-band measurements with a common TX/RX setup in the same environment. Figs. 4(a) and 4(b) show the blockage loss, with mean loss, 95% confidence intervals, along with a linear regression fit to the measured blockage loss having slope parameter α and intercept β. The figures show that the measured data samples are not large enough to provide enough degrees of freedom to draw statistically significant conclusions. Therefore, we conduct p-value tests to investigate the validity of null hypothesis, with $\alpha = 0$ meaning that there exists no statistically significant frequency trend. We assume a p-value threshold, i.e., $p \leq 0.05$ to demonstrate that the frequency

trend is statistically significant. In addition to the p-value test, we also conduct an R-square test in order to analyze the goodness of linear regression fit. In our analysis, linear regression fits pass the goodness of fit test if R-square value is greater than 0.8.
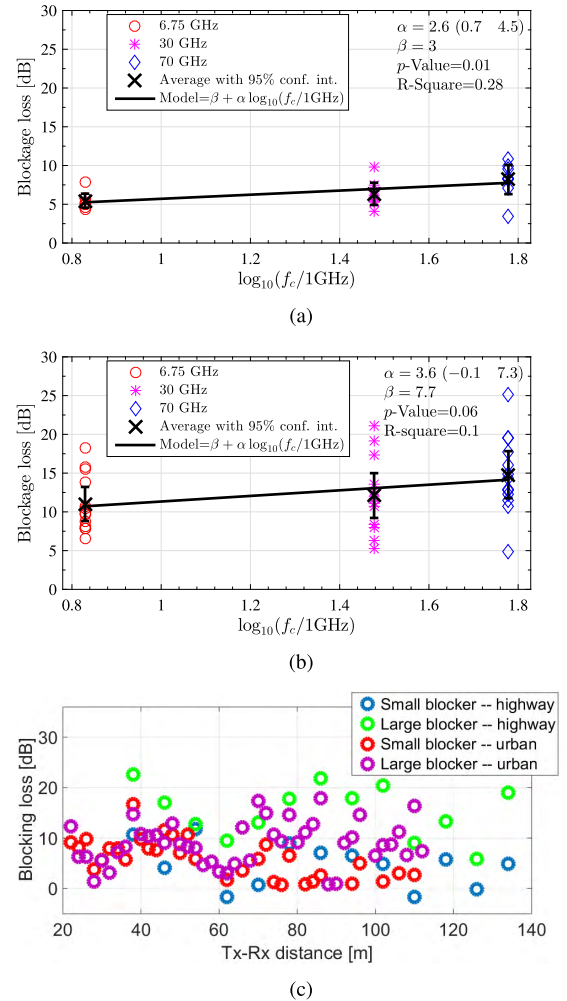
Results in Fig. 4(a) and Fig. 4(b) demonstrate p-values of 0.01 and 0.06 for the small and large blocker case, respectively. This shows that frequency dependency of blockage loss is statistically significant in case of small blocking vehicle and quasi-significant in case of large blocking vehicle. Therefore, we can reject the null hypothesis as the increase in blockage loss with frequency is statistically significant. Results in Fig. 4(a) and Fig. 4(b) also indicate that linear regression fits do not pass the goodness of fit test due small R-square values. This is due to large standard deviations in the blockage loss at the measured positions for different frequency bands. From the low p-value and R-square values, we conclude that, even though there is significant variability of blockage loss at different positions the blocking vehicle (both large and small), the basic trend of higher loss with increasing frequency holds. Comparing the linear fits for small and large blocking vehicles, both the base loss and the slope are higher for the large blocker. Furthermore, the frequency-dependent slope in both cases, while existent, is not very steep, thus showing that V2V communication is feasible in higher frequencies even under vehicle blockage.

Theoretical and measurement studies indicate that vehicle blockage loss reduces with an increase in TX-RX distance [24], [37]. To evaluate if blockage loss is significant for mmWave V2V channels at the longer TX-RX distances, we characterize the blockage loss with respect to the distance between TX and RX using the 73 GHz measurements in Chengdu Highway and Urban scenarios. Fig. 4(c) shows the
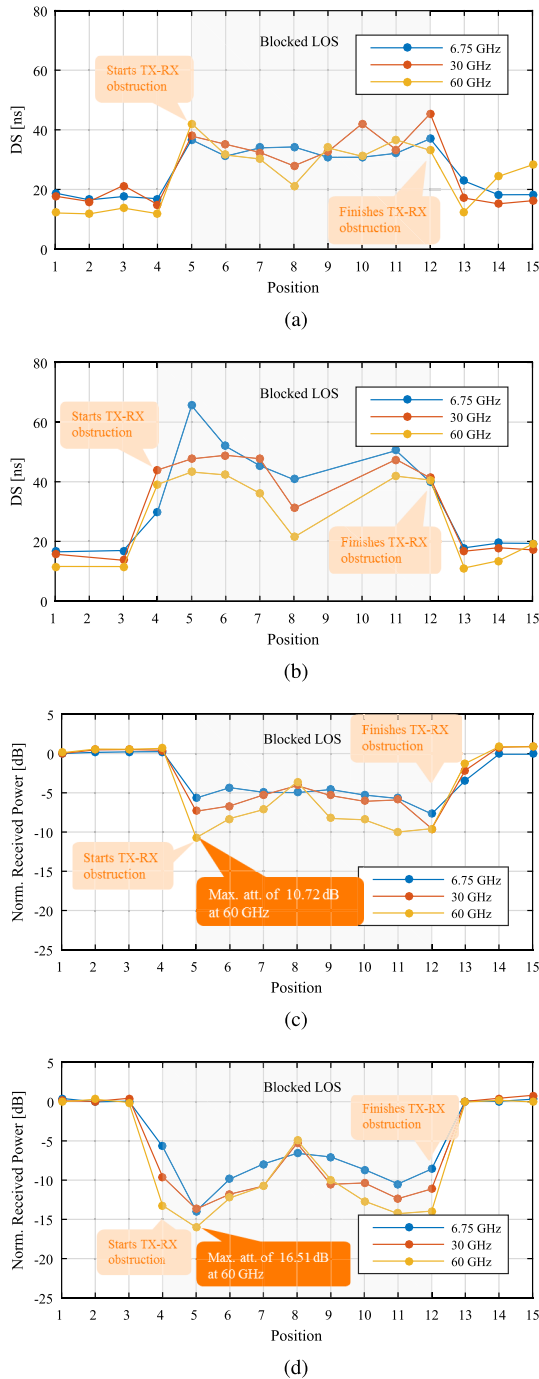
FIGURE 3. Per-position received power and Delay Spread in Ilmenau Urban scenario. (a) Delay Spread per position, small blocker. (b) Delay Spread per position, large blocker. (c) Received power per position, small blocker. (d) Received power per position, large blocker.

FIGURE 4. Blockage loss analysis as a function of frequency and blocker size– subfigures (a) and (b), the additional loss is with respect to measurements without the blocking vehicle in any of the positions in Fig. 1(a). In Chengdu Highway and Urban scenarios (subfigure (c)), the additional loss per point is with respect to the LOS measurement in the same location and at the same distance between TX and RX.

distance dependent blockage loss for highway and urban scenarios with a small and large blocker. Several observations can be made: i) blockage loss in the urban and highway scenarios is comparable, with similar results for the same blocker size (Table 1); ii) while decreasing, the blockage loss persists over increasing TX-RX distances (e.g., a large blocker occasionally introduces 20 dB loss over 130 m distance in highway), thus showing that the vehicle blockage is important

even over large communication distances; and iii) the size of a blocker plays a major role in both highway and urban scenarios, with large blocker introducing on average 6 dB additional loss (Table 1). Since 120° HPBW antennas were used in Chengdu scenarios, we can consider these results as representative of "application-specific" antenna configurations (e.g., transmissions to the front and rear vehicles in the platooning use case [1]). The results further indicate that directional transmissions between vehicles would benefit from advanced transmissions techniques (e.g., beamforming), in order to reduce the effect of blockage loss by focusing transmission along the dominant multipaths. Finally, a more comprehensive analysis is required to fully characterize the effect of distance on the additional blockage loss, including at least: i) multiple blockers; ii) multiple locations of blocking vehicles relative to transmitter and receiver; and iii) larger TX-RX distances to account for all advanced use cases, some of which require 1000 m range [47].
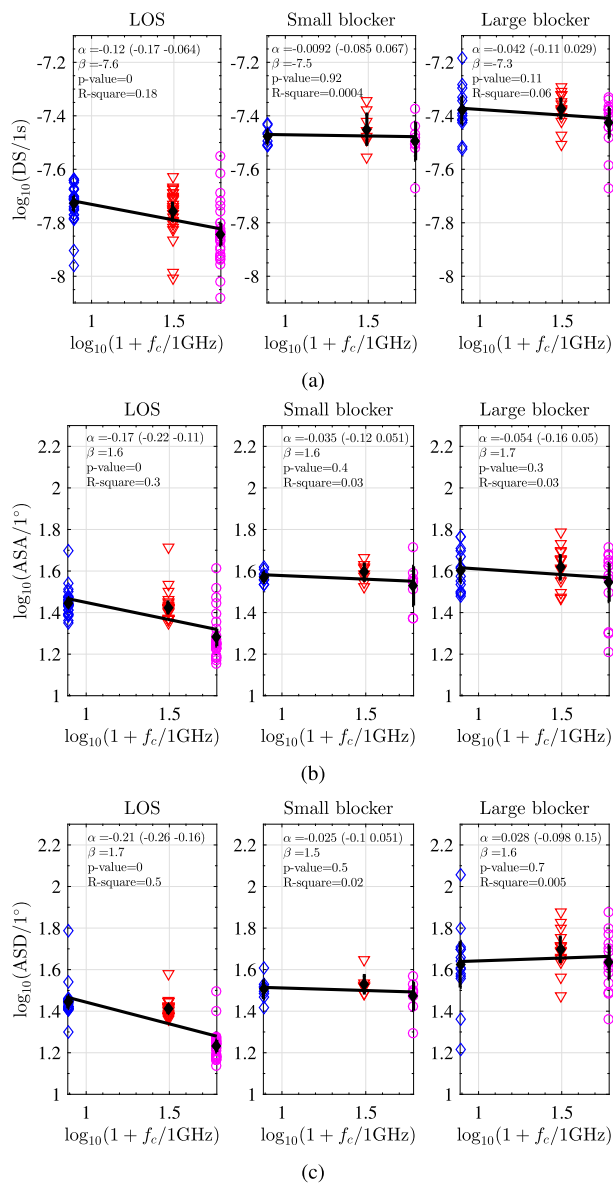
FIGURE 5. Fast fading parameter analysis as a function of frequency and blocker size for a synthesized omni-directional channel. (a) RMS delay spread vs frequency – Ilmenau Urban. (b) ASA vs frequency – Ilmenau Urban. (c) ASD vs vs frequency – Ilmenau Urban.

E. FREQUENCY DEPENDENCY OF FAST FADING PARAMETERS

Frequency dependence of the mmWave propagation channels is a question of continued interest. Recently, an extensive study of channels measured at 6-100 GHz as a part of the mmMAGIC project [48] concluded that a relationship between the carrier frequency and the fast fading parameters is hard to define. In our measurement campaign performed in Ilmenau, we followed the same guidelines used in [48] for the inter-band comparison. The results in Fig. 5 show linear fits of the measured fast fading parameters compared to the 3GPP model [49]:

$$\mu_{\log \text{DS}/1s, \text{ASA}/1°, \text{ASD}/1°} = \alpha \log \left(1 + f_c/1\text{GHz}\right) + \beta \quad (2)$$

Similar to the blockage loss model in Section III-C, we assume null hypothesis $\alpha = 0$ for the model in (2). The goodness of the model fit is analyzed by R-square test. From Fig. 5, it is interesting to note that null hypothesis can be rejected in LOS case for both delay and angular dispersion statistics due to the very small p-values. However, similar to blockage loss model in Section III-C, the model in (2) does not pass goodness of the fit test due to the large variations in the delay and angular dispersion statistics. Despite this fact, we can still conclude that in the LOS case the model in (2) is still useful in the sense that measurements demonstrate clear trend with an increase in frequency.

Fig. 5 shows the dispersion statistics when LOS path is obstructed by a small or a large blocking vehicle. In contrast to the LOS scenario, the null hypothesis cannot be rejected due to large p-values, i.e., greater than 0.05. Additionally, neither of the results in LOS path blockage scenario pass the goodness of fit test. These results demonstrate that, if LOS path is obstructed, frequency dependence of fast fading parameters as explained by the model in (2) is hard to establish. The results in Table 1 also show that the increased blocker size results in not only higher blockage losses, but also more pronounced delay and angular spreads. As expected, the directional channel measurement results shown in Table 1 demonstrate lower DS values than omni-directional channels. This is quite an intuitive result, since with 120° HPBW antennas there is a spatially filtered multi-path channel. However, in the Chengdu urban scenario in the 73 GHz band, the increased angular spreads in case of directional measurements compared to omni-directional channels (at lower frequency bands) are counter-intuitive. However, since they correspond to different scenarios, it is difficult to make a representative comparison due to the intrinsic differences that arise in the environments shown in Fig. 1. Furthermore, due to the 30° HPBW antennas, the angular estimate of the multi-path components is coarse. Therefore, an exact explanation of this observation is not possible. However, a possible explanation comes from the environment itself shown in Fig. 1(b), where reflected multipath components from the cars on the left and the building on the right side of the blocking vehicle may roughly exhibit similar propagation distances, while being widely separated in space and thus in terms of angles. In contrast to the Chengdu Urban scenario, delay and angular spread values for the blocked LOS in the Chengdu Highway scenario are quite consistent with the omni-directional channels, where one expects reduced delay and angular spreads when a blocker screens out many angles.

F. ANGULAR DOMAIN ANALYSIS

As discussed in Section I, the use of low antennas in the V2V communication results in a significantly more cluttered propagation channel than that of a typical cellular uplink/downlink. V2V communication results in a rich multipath scattering on both ends of the link. Consequently, there is broad and comparable angular spread at both the
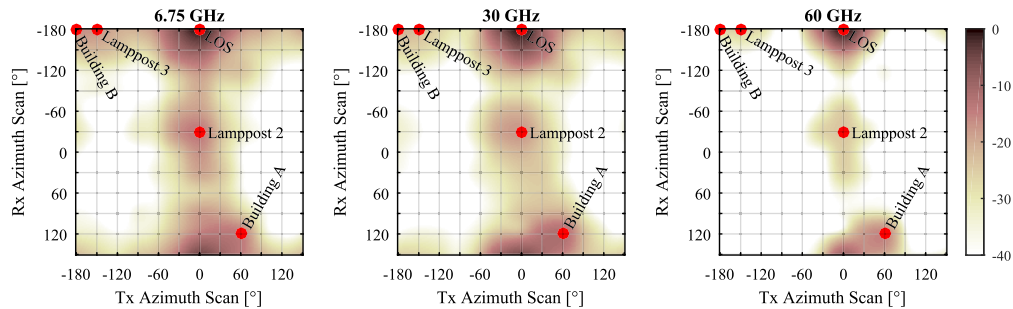
FIGURE 6. Power bi-azimuthal profile in Ilmenau Urban, large blocker scenario, Position 8 from Fig. 1(a).

TX (departure) and RX (arrival) side. We investigated the angular characteristics across frequencies in the Ilmenau Urban scenario by analyzing the interpolated power bi-azimuth profile for Position 8, as shown in Fig. 6. The bi-azimuth profile is calculated by integrating the PDP measured at every TX and RX scanning direction. Each plot in Fig. 6 is normalized by the suprema of the corresponding bi-azimuth power angular profile. It is important to point out that, since the antennas were not de-embedded, even if they have a very similar pattern in the different bands, the results are still shaped by them. The figure shows how the sparsity of the channel in the angular domain increases with the carrier frequency. This increase is a result of a larger number of scatterers available at lower frequencies (as seen in Fig. 2). Even though the strongest components are located in the LOS directions, we can see a wide distribution of the remaining scatterers over almost the whole azimuth plane at TX and RX, demonstrating a rich multipath environment. The impact of the different blocking vehicle positions in the directional domain and obstruction of the different scatterers can be seen in the transition from the Position 4 to Position 5, also analyzed in the time domain in Fig. 2. It can be observed that, while sparser, the mmWave channels still retain the most dominant scatterers observed at 6.75 GHz, albeit with different power contributions. The diffuse/weak scatterers vanish below the dynamic threshold due to increased attenuation loss at the mmWave frequency bands. For the large blocker case, this may result in reducing the average delay and angular spreads with the carrier frequency as shown in Table 1. For example, in Position 5, the power of the LOS component at 6.75 GHz is similar to the other scatterers (likely a result of less attenuated penetration through the vehicle). However, at 30 GHz and 60 GHz, the LOS component is more attenuated (due to higher penetration loss) and reflections are the strongest components.

We note that our measurements were performed with a fairly coarse angular resolution and specific MPC could be better identified with finer resolution measurements. However, the distribution in both the azimuth of the TX and of the RX (Fig. 6) shows a large angular distribution, which holds irrespective of the coarseness of the angular resolution and is a result of a rich scattering environment.

IV. CONCLUSIONS

We performed multi-band (6.75 GHz, 30 GHz, 60 GHz, 73 GHz) V2V channel measurements and parameterization in urban and highway scenarios in Germany and China, with the focus on the impact of vehicle blockage. Two types of vehicle blockers were investigated: small blocker (personal vehicle) and large blocker (van, bus). The results show that blockage loss is significantly impacted by blocker size, with values increasing from 5.5 dB-8.2 dB in case of small blocker to 8.2 dB-17 dB in case of large blocker. In addition to blockage loss, vehicle blockage considerably increases delay and angular spreads. By combining the larger bandwidth that is typically available in the mmWave bands compared to lower frequencies and by employing efficient beamforming techniques, our results indicate that *V2V communication in mmWaves will be possible, even if the LOS path is obstructed by vehicles*. We base this conclusion on the following technical and practical arguments.

- Virtually all significant specular reflections in 6.75 GHz band are available in both mmWave bands (30 GHz, 60 GHz), as shown in Fig. 2.
- The normalized received power at 6.75 GHz is at most 8 dB higher than in mmWave bands in any of the blocker positions (see Fig. 4 and Table 1). In certain scenarios (e.g., when the blocker is in the middle between TX and RX), the normalized received power is even higher at mmWaves than at 6.75 GHz (Fig. 3). This is in contrast with previous research that showed higher loss in mmWaves, which was a result of channel measurements with directional antennas, and not the effect of the channel itself.
- Angular spreads, while reducing with increasing frequency, are doing so with a gentle slope (Fig 5 and Table 1).
- Given the physical size of the antennas, larger number of antennas is feasible in the mmWave bands. For example, up to 32 TX/RX antenna elements are assumed for mmWaves in [49], compared to up to 8 for below 6 GHz bands. The increased number of antennas will help compensate the increased blockage loss at higher frequencies.

Considerably larger bandwidth is typically available in the mmWave bands. For example, compared to the 30 MHz bandwidth allocated for V2V in 5.9 GHz band in Europe, a total of one GHz is available for V2V in the 63-64 GHz band. Higher bandwidth will allow for a comparable or even a higher throughput in certain scenarios.

Several salient aspects need to be further studied to fully characterize V2V channels above 6 GHz. Since lower location of antennas on vehicles is going to result in the change of blockage loss and delay and angular spreads, characterization of V2V channels for antenna locations on vehicle other than roof-level (e.g., bumper-level or side mirror) is necessary. Furthermore, sufficient measurements at different TX-RX distances are necessary to derive new path loss equations for V2V channels under LOS and due to vehicle and building blockage. Finally, measurements and modeling in mobile environment (in terms of the mobility of TX, RX, and surrounding vehicles) are necessary to characterize Doppler effect for mmWave V2V channels.

REFERENCES

[1] *Study Enhancement 3GPP Support for 5G V2X Services (Release 15)*, document 3GPP TR 22.886 v15.1.0, 3GPP, Mar. 2017.
[2] M. Boban, A. Kousaridas, K. Manolakis, J. Eichinger, and W. Xu, "Connected roads of the future: Use cases, requirements, and design considerations for vehicle-to-everything communications," *IEEE Veh. Technol. Mag.*, vol. 13, no. 3, pp. 110–123, Sep. 2018.
[3] W. Viriyasitavat, M. Boban, H.-M. Tsai, and A. Vasilakos, "Vehicular communications: Survey and challenges of channel and propagation models," *IEEE Veh. Technol. Mag.*, vol. 10, no. 2, pp. 55–66, Jun. 2015.
[4] A. F. Molisch, F. Tufvesson, J. Kåredal, and C. F. Mecklenbräuker, "A survey on vehicle-to-vehicle propagation channels," *IEEE Commun. Mag.*, vol. 16, no. 6, pp. 12–22, Dec. 2009.
[5] D. W. Matolak, "V2V communication channels: State of knowledge, new results, and what's next," in *Proc. Int. Workshop Commun. Technol. Vehicles*. Berlin, Germany: Springer, 2013, pp. 1–21.
[6] J. Maurer, T. Fugen, T. Schafer, and W. Wiesbeck, "A new inter-vehicle communications (IVC) channel model," in *Proc. IEEE 60th Veh. Technol. Conf. (VTC-Fall)*, vol. 1, Sep. 2004, pp. 9–13.
[7] L. Cheng, B. E. Henty, D. D. Stancil, F. Bai, and P. Mudalige, "Mobile vehicle-to-vehicle narrow-band channel measurement and characterization of the 5.9 GHz dedicated short range communication (DSRC) frequency band," *IEEE J. Sel. Areas Commun.*, vol. 25, no. 8, pp. 1501–1516, Oct. 2007.
[8] I. Sen and D. W. Matolak, "Vehicle–vehicle channel models for the 5-GHz band," *IEEE Trans. Intell. Transp. Syst.*, vol. 9, no. 2, pp. 235–245, Jun. 2008.
[9] J. Karedal *et al.*, "A geometry-based stochastic MIMO model for vehicle-to-vehicle communications," *IEEE Trans. Wireless Commun.*, vol. 8, no. 7, pp. 3646–3657, Jul. 2009.
[10] J. Turkka and M. Renfors, "Path loss measurements for a non-line-of-sight mobile-to-mobile environment," in *Proc. 8th Int. Conf. ITS Telecommun.*, Oct. 2008, pp. 274–278.
[11] C. F. Mecklenbrauker *et al.*, "Vehicular channel characterization and its implications for wireless system design and performance," *Proc. IEEE*, vol. 99, no. 7, pp. 1189–1212, Jul. 2011.
[12] X. Cai, B. Peng, X. Yin, and A. P. Yuste, "Hough-transform-based cluster identification and modeling for V2V channels based on measurements," *IEEE Trans. Veh. Technol.*, vol. 67, no. 5, pp. 3838–3852, May 2018.
[13] E. Giordano, R. Frank, G. Pau, and M. Gerla, "CORNER: A realistic urban propagation model for VANET," in *Proc. 7th Int. Conf. Wireless Demand Netw. Syst. Services (WONS)*, Feb. 2010, pp. 57–60.
[14] T. Mangel, O. Klemp, and H. Hartenstein, "A validated 5.9 GHz non-line-of-sight path-loss and fading model for inter-vehicle communication," in *Proc. 11th Int. Conf. ITS Telecommun.*, Aug. 2011, pp. 75–80.

[15] P. Paschalidis, K. Mahler, A. Kortke, M. Peter, and W. Keusgen, "Pathloss and multipath power decay of the wideband car-to-car channel at 5.7 GHz," in *Proc. IEEE 73rd Veh. Technol. Conf. (VTC Spring)*, May 2011, pp. 1–5.
[16] K. Mahler, P. Paschalidis, M. Wisotzki, A. Kortke, and W. Keusgen, "Evaluation of vehicular communication performance at street intersections," in *Proc. IEEE 80th Veh. Technol. Conf. (VTC-Fall)*, Sep. 2014, pp. 1–5.
[17] Z. Xu *et al.*, "Relaying for ieee 802.11p at road intersection using a vehicular non-stationary channel model," in *Proc. IEEE 6th Int. Symp. Wireless Veh. Commun. (WiVeC)*, Sep. 2014, pp. 1–6.
[18] O. Onubogu, K. Ziri-Castro, D. Jayalath, K. Ansari, and H. Suzuki, "Empirical vehicle-to-vehicle pathloss modeling in highway, suburban and urban environments at 5.8 GHz," in *Proc. 8th Int. Conf. Signal Process. Commun. Syst. (ICSPCS)*, Dec. 2014, pp. 1–6.
[19] L. Urquiza-Aguiar, C. Tripp-Barba, J. Estrada-Jiménez, and M. A. Igartua, "On the impact of building attenuation models in VANET simulations of urban scenarios," *Electronics*, vol. 4, no. 1, pp. 37–58, 2015.
[20] R. Meireles, M. Boban, P. Steenkiste, O. Tonguz, and J. Barros, "Experimental study on the impact of vehicular obstructions in VANETs," in *Proc. IEEE Veh. Netw. Conf. (VNC)*, Dec. 2010, pp. 338–345.
[21] M. Boban, T. T. V. Vinhoza, M. Ferreira, J. Barros, and O. K. Tonguz, "Impact of vehicles as obstacles in vehicular ad hoc networks," *IEEE J. Sel. Areas Commun.*, vol. 29, no. 1, pp. 15–28, Jan. 2011.
[22] T. Abbas, K. Sjöberg, J. Karedal, and F. Tufvesson, "A measurement based shadow fading model for vehicle-to-vehicle network simulations," *Int. J. Antennas Propag.*, vol. 2015, May 2015, Art. no. 190607.
[23] M. G. Nilsson, C. Gustafson, T. Abbas, and F. Tufvesson, "A measurement-based multilink shadowing model for V2V network simulations of highway scenarios," *IEEE Trans. Veh. Technol.*, vol. 66, no. 10, pp. 8632–8643, Oct. 2017.
[24] R. He, A. F. Molisch, F. Tufvesson, Z. Zhong, B. Ai, and T. Zhang, "Vehicle-to-vehicle propagation models with large vehicle obstructions," *IEEE Trans. Intell. Transp. Syst.*, vol. 15, no. 5, pp. 2237–2248, Oct. 2014.
[25] *Revision of SI: Study on Evaluation Methodology of New V2X Use Cases for LTE and NR (Release 15)*, document RP-171093, 3GPP, Jun. 2017.
[26] M. G. Sánchez, M. P. Táboas, and E. L. Cid, "Millimeter wave radio channel characterization for 5g vehicle-to-vehicle communications," *Measurement*, vol. 95, pp. 223–229, Jan. 2017.
[27] A. Kato, K. Sato, M. Fujise, and S. Kawakami, "Propagation characteristics of 60-GHz millimeter waves for ITS inter-vehicle communications," *IEICE Trans. Commun.*, vol. 84, no. 9, pp. 2530–2539, 2001.
[28] K. Sato and M. Fujise, "Propagation measurements for inter-vehicle communication in 76-GHz band," in *Proc. 6th Int. Conf. ITS Telecommun.*, Jun. 2006, pp. 408–411.
[29] S. Takahashi, A. Kato, K. Sato, and M. Fujise, "Distance dependence of path loss for millimeter wave inter-vehicle communications," in *Proc. IEEE Veh. Technol. Conf. (VTC-Fall)*, Oct. 2003, pp. 26–30.
[30] J.-J. Park, J. Lee, J. Liang, K.-W. Kim, K.-C. Lee, and M.-D. Kim, "Millimeter wave vehicular blockage characteristics based on 28 GHz measurements," in *Proc. IEEE Veh. Technol. Conf. (VTC-Fall)*, Sep. 2017, pp. 1–5.
[31] A. Yamamoto, K. Ogawa, T. Horimatsu, A. Kato, and M. Fujise, "Path-loss prediction models for intervehicle communication at 60 GHz," *IEEE Trans. Veh. Technol.*, vol. 57, no. 1, pp. 65–78, Jan. 2008.
[32] K. Sato, M. Fujise, R. Tachita, E. Hase, and T. Nose, "Propagation in ROF road-vehicle communication system using millimeter wave," in *Proc. IEEE Int. Vehicle Electron. Conf. (IVEC)*, Sep. 2001, pp. 131–135.
[33] V. Semkin, U. Virk, A. Karttunen, K. Haneda, and A. V. Räisänen, "E-band propagation channel measurements in an urban street canyon," in *Proc. 9th Eur. Conf. Antennas Propag. (EuCAP)*, May 2015, pp. 1–4.
[34] P. Okvist *et al.*, "15 GHz street-level blocking characteristics assessed with 5G radio access prototype," in *Proc. IEEE 83rd Veh. Technol. Conf. (VTC Spring)*, May 2016, pp. 1–5.
[35] C. U. Bas *et al.* (2017). "Dynamic double directional propagation channel measurements at 28 GHz." [Online]. Available: https://arxiv.org/abs/1711.00169
[36] M. Boban, X. Gong, and W. Xu, "Modeling the evolution of line-of-sight blockage for V2V channels," in *Proc. IEEE Veh. Technol. Conf. (VTC-Fall)*, Jun. 2016, pp. 1–7.
[37] M. Boban, J. Barros, and O. K. Tonguz, "Geometry-based vehicle-to-vehicle channel modeling for large-scale simulation," *IEEE Trans. Veh. Technol.*, vol. 63, no. 9, pp. 4146–4164, Nov. 2014.
[38] D. Dupleich *et al.*, "Multi-band spatio-temporal characterization of a V2V environment under blockage," in *Proc. 12th Eur. Conf. Antennas Propag. (EuCAP)*, 2018, p. 5.

[39] D. Dupleich *et al.*, "Investigations on fading scaling with bandwidth and directivity at 60 GHz," in *Proc. 11th Eur. Conf. Antennas Propag. (EuCAP)*, Paris, France, 2017, pp. 3375–3379.

[40] N. Iqbal *et al.*, "Second-order statistical characterization of the 60 GHz cluster fading channels," in *Proc. IEEE 29th Annu. Int. Symp. Pers., Indoor, Mobile Radio Commun. (PIMRC), Workshop WS Millimiter Waves Commun. (IEEE PIMRC Workshop (WS)*, Bologna, Italy, Sep. 2018, pp. 241–245.

[41] R. Müller, R. Herrmann, D. A. Dupleich, C. Schneider, and R. S. Thomä, "Ultrawideband multichannel sounding for mm-Wave," in *Proc. 8th Eur. Conf. Antennas Propag. (EuCAP)*, 2014, pp. 817–821.

[42] R. Müller *et al.*, "Simultaneous multi-band channel sounding at mm-Wave frequencies," in *Proc. 10th Eur. Conf. Antennas Propag. (EuCAP)*, 2016, pp. 1–5.

[43] S. Sun, G. R. MacCartney, Jr., M. K. Samimi, and T. S. Rappaport. (2015). "Synthesizing omnidirectional antenna patterns, received power and path loss from directional antennas for 5G millimeter-wave communications." [Online]. Available: https://arxiv.org/abs/1511.07271

[44] K. Haneda, S. L. H. Nguyen, J. Järveläinen, and J. Putkonen, "Estimating the omni-directional pathloss from directional channel sounding," in *Proc. 10th Eur. Conf. Antennas Propag. (EuCAP)*, Apr. 2016, pp. 1–5.

[45] W. Q. Malik, D. J. Edwards, and C. J. Stevens, "Frequency dependence of fading statistics for ultrawideband systems," *IEEE Trans. Wireless Commun.*, vol. 6, no. 3, pp. 800–804, Mar. 2007.

[46] A. Böttcher, C. Schneider, P. Vary, and R. S. Thomä, "Dependency of the power and delay domain parameters on antenna height and distance in urban macro cell," in *Proc. 5th Eur. Conf. Antennas Propag. (EUCAP)*, 2011, pp. 1395–1399.

[47] *Service Requirements for Enhanced V2X Scenarios (Release 15)*, document 3GPP TR 22.186 V15.0.0, 3GPP, Mar. 2017.

[48] S. L. H. Nguyen *et al.*, "On the frequency dependency of radio channel's delay spread: Analyses and findings from mmMAGIC multi-frequency channel sounding," in *Proc. 12th Eur. Conf. Antennas Propag. (EuCAP)*, London, U.K., Apr. 2018, pp. 634–638.

[49] *Study on Evaluation Methodology of New Vehicle-to-Everything V2X Use Cases for LTE and NR*, document 3GPP TR 37.885 V15.1.0, 3rd Generation Partnership Project, 2018.

MATE BOBAN received the Diploma degree in informatics from the University of Zagreb, Croatia, and the Ph.D. degree in electrical and computer engineering from Carnegie Mellon University, Pittsburgh, PA, USA, in 2004 and 2012, respectively. He is a Principal Research Engineer with Huawei Munich Research Center, Germany. Before joining Huawei, he was with NEC Labs Europe, Carnegie Mellon University, and Apple. He is an Alumnus of the Fulbright Scholar Program. He has co-chaired several IEEE workshops and conferences and has been involved in European Union-funded projects on vehicle-to-everything (V2X) communication (5G-CAR, DRIVE-C2X, and TEAM) as a Work Package Leader and editor of deliverables. He actively participates in key industry and standardization bodies dealing with V2X: 3GPP, 5GAA, and ETSI. His current research interests include channel modeling, resource allocation, and machine learning applied to V2X communication systems. For his work on V2X, he received the Best Paper Awards at the IEEE Vehicular Technology Conference and the IEEE Vehicular Networking Conference.

DIEGO DUPLEICH received the Engineering degree in electronic engineering from Universidad Tecnológica Nacional, Paraná, Argentina, in 2009, and the M.Sc. degree (Hons.) in communications and signal processing from Technische Universität at Ilmenau, Ilmenau, Germany, in 2013, where he is currently pursuing the Ph.D. degree in electrical engineering. From 2009 to 2010, he was an RF Specialist in satellite communications with Emerging Markets Communications, Raisting, Germany. Since 2013, he has been with the Electronic Measurement Research Laboratory, Technische Universität at Ilmenau, where he is currently involved in the millimeter-wave field.

NAVEED IQBAL received the M.Sc. degree in communications and signal processing from Technische Universität at Ilmenau, Germany. He is currently pursuing the Ph.D. degree with the Huawei Technologies Research Center, Munich, Germany. His research interests include channel measurements/ modeling for millimeter-wave systems, deterministic and randomized antenna selection algorithms, as well as beamforming techniques for MIMO systems. He has co-authored two best research award-winning papers in the European Wireless Conference, in 2013, and the European Conference of Antennas and Propagation, in 2017.

JIAN LUO received the B.A.Sc. degree in communication engineering from the South China University of Technology, Guangzhou, China, in 2004, and the M.S. and Ph.D. degrees in electrical engineering from Technische Universität at Berlin, Berlin, Germany, in 2006 and 2012, respectively. From 2007 to 2012, he was a Researcher with the Fraunhofer Heinrich Hertz Institute, Berlin, and was involved in several German national and EU funded projects, e.g., EASY-A, SMART-RF, and SAPHYRE. Since 2012, he has been with the German Research Center, Huawei Technologies Duesseldorf GmbH, Duesseldorf, Germany, where he is involved in 5G wireless communication systems. He has been involved in EU 5GPPP projects, METIS and mmMAGIC, where he has been leading the air-interface design. His current research interests include millimeter (mm)-wave channel measurement and modeling and mm-wave communication system design.

CHRISTIAN SCHNEIDER received the Diploma degree in electrical engineering from Technische Universität at Ilmenau, Ilmenau, Germany, in 2001, where he is currently pursuing the Ph.D. degree with the Institute for Information Technology. His current research interests include wireless multidimensional channel sounding, channel characterization and analysis, channel modeling for single-link and multilink cases in cellular and vehicular networks at microwave and millimeter-wave bands, space–time signal processing, adaptive techniques, and passive coherent localization. He was a recipient of the Best Paper Award at the European Wireless Conference, in 2013, and the European Conference of Antennas and Propagation, in 2017.

ROBERT MÜLLER received the M.S. degree in electronic engineering from the Berlin University of Technology, Berlin, Germany, in 2009. His research interest includes high-frequency component design. Furthermore, he is also involved in high-frequency front-end design, antenna design, ultrawideband system design, and special antenna array design for channel sounding applications. His current research interest includes channel sounding measurement system and analysis for a further communication system in the field of V2V and cellular networks.

ZIMING YU received the B.S. degree in telecommunication from Jiangxi University of Science and Technology, Jiangxi, China, in 2005, and the M.S. degree in mobile communication from Chongqing University of Posts and Telecommunications, Chongqing, China, in 2009. He joined Huawei Technologies Co., Ltd, Chengdu, China, in 2012. His research interests include millimeter wave channel measurement, sounder system design and channel modeling. His current research interests include the V2V propagation channel, foliage attenuation, body network and Terahertz propagation channel.

DAVID STEER received degrees in physics and electrical engineering from Queen's University, Kingston, ON, Canada, in 1972 and 1974, respectively, and the Ph.D. degree in radio astronomy from the University of British Columbia, in 1984. He is currently a Staff Engineer with the Huawei Canada Research Centre, Kanata, ON, Canada. He began his communications career in the days of cross-bar voice circuit switching at Bell-Northern Research, in 1974. Since then, his work has included communications security systems, personal radio communications, 3GPP/ETSI standards, spectrum management, and latterly mm-wave technology for mobile systems. In this process, he became a named inventor for some 100 issued patents for communications. His current research interests include the physics of mm-wave channel modeling, spectrum management, and radio technology for next-generation mobile systems. He is a Life Member of the IEEE.

TOMMI JÄMSÄ graduated from Oulu University, in 1995. During his career at Elektrobit and Anite Telecoms, from 1993 to 2015, his responsibilities have been product management, radio channel research, and standardization. He has contributed channel models and test methodologies to several international fora and projects, such as COST, WiMAX, 3GPP, ITU-R, WINNER, and METIS. Currently, he is a Consultant with Tommi Jamsa Consulting and acts as a Senior Expert in channel modeling with Huawei Technologies, Sweden.

JIAN LI received the Ph.D. degree from Fudan University, in 2006. From 2006 to 2007, he was with the Chinese Academy of Science. In 2007, he was a Senior Strategy Research Engineer with Alcatel-Lucent. He joined the 2012 Lab of Huawei, in 2011. Since 2017, he has been the Director of the 5G Research Lab, Munich Research Center of Huawei. He has contributed to the 3GPP and ITU-R standard for 5G channel modeling. His research interests include NR V2X, industrial IoT, and channel modeling for MIMO and mm-wave bands.

REINER S. THOMÄ (M'92–SM'99–F'07) received the Dipl.Ing. (M.S.E.E.), Dr.Ing. (Ph.D.E.E.), and Dr.Ing.Habil. degrees in electrical engineering and information technology from Technische Hochschule Ilmenau, Ilmenau, Germany, in 1975, 1983, and 1989, respectively, where he was a Research Associate in electronic circuits, measurement engineering, and digital signal processing, from 1975 to 1988. From 1988 to 1990, he was a Research Engineer with the Akademie der Wissenschaften der DDR (Zentrum für Wissenschaftlichen Gerätebau), Berlin, Germany, where he was involved in radio surveillance. In 1991, he spent a sabbatical leave at the University of Erlangen–Nürnberg (Lehrstuhl für Nachrichtentechnik), Erlangen, Germany. Since 1992, he has been a Professor of electrical engineering (electronic measurement) with TU Ilmenau, where he was the Director of the Institute of Communications and Measurement Engineering, from 1999 to 2005. With his group, he has contributed to several European and German research projects and clusters, such as RESCUE, WINNER, PULSERS, EUWB, NEWCOM, COST 273, 2100, IC 1004, COST IRACON, EASY-A, and EASY-C. He was the Speaker of the German nation-wide DFG-focus project, Ultra-Wideband Radio Technologies for Communications, Localization, and Sensor Applications (SPP 1202). His current research interests include measurement and digital signal processing methods (correlation and spectral analysis, system identification, sensor arrays, compressive sensing, and time–frequency and cyclostationary signal analysis), their application in mobile radio and radar systems (multidimensional channel sounding, propagation measurement and parameter estimation, and MIMO-, mm-wave-, and ultrawideband radar), measurement-based performance evaluation of MIMO transmission systems, including over-the-air testing in virtual electromagnetic environments, passive coherent location, and UWB radar sensor systems for object detection, tracking, and imaging. He is a member of URSI (Comm. A), VDE/ITG. He was an Advisory Board Member of EU project—mmMAGIC. Since 1999, he has been the Chair of the IEEE-IM TC-13 on Measurement in Wireless and Telecommunications. He was a recipient of the Thuringian State Research Award for Applied Research for contributions to high-resolution multidimensional channel sounding, in 2007, and the Vodafone Innovation Award, in 2014.

● ● ●